

Article

# The Effect of the Linking Unit on the Electronic and Magnetic Interactions in Copper(II) Porphyrin Dimers Linked by Metal Ions

Jordan L. Appleton, Nolwenn Le Breton, Sylvie Choua \* and Romain Ruppert \* 

Institut de Chimie, UMR CNRS 7177, Université de Strasbourg, 4 Rue Blaise Pascal, 67000 Strasbourg, France; jappleton@unistra.fr (J.L.A.); nlebreton@unistra.fr (N.L.B.)

\* Correspondence: sylvie.choua@unistra.fr (S.C.); ruppert@unistra.fr (R.R.)

**Abstract:** The syntheses of a series of copper(II) porphyrins and their dimers linked by palladium(II) or platinum(II) are reported. Their electronic properties and their magnetic properties were studied. In particular, the effect of the linking unit on these properties was evaluated. It was discovered that three factors influence the electronic and magnetic interactions between the two metalloporphyrins: the nature of the linking metal ion, the nature of the external coordination site of the porphyrin, and also the nature of the metal ion present in the central core of the aromatic macrocycle.

**Keywords:** porphyrinoids; magnetic interactions; electronic delocalization; electrochemistry

## 1. Introduction

Macrocyclic compounds as ligands have been developed by inorganic chemists to encapsulate different metal ions with large binding constants. Aromatic macrocycles, particularly porphyrinoid compounds, have been prepared in recent decades due to their inspiring biological role in obtaining new molecules or even materials with interesting optical, electronic, or magnetic properties [1]. Their photophysical properties have been used for applications in photodynamic therapy or dye-sensitized solar cells [2–6]. For many biological applications, the extension of the aromatic core to improve the chromophores and/or the syntheses of larger oligoporphyrins for materials applications has led to a development of the synthetic methodologies used to prepare larger molecules and the analytical tools to study their properties [7,8]. The study of porphyrinoid dimers and even higher homologues was initiated in order to mimic the properties of natural systems like the photosynthetic reaction center (light harvesting and light conversion to chemical energy) [9]. These syntheses of porphyrinoid dimers led quite rapidly to the development of molecules designed to obtain new materials with interesting electronic and magnetic properties. Electronic delocalization over large areas was reached by conjugation between the aromatic subunits [10–15], and this approach was extremely successful, with the synthesis of chromophores reaching far into the infrared domain [16]. Some examples of porphyrin dimers are represented in Figure 1, with covalent linkages, conjugated or not, and triply fused to obtain the most efficient electronic delocalization. Similar molecules were developed to study the magnetic interactions between two paramagnetic centers separated by rather long distances [17–24]. Apart from porphyrin dimers, porphyrazines and phthalocyanines [25–29] were also modified to create compounds containing two paramagnetic metal ions. More recently, vanadyl porphyrins or vanadyl porphyrin dimers were proposed as potential species in the field of molecular quantum technologies. Such quantum technologies would be able to outperform classical computers in some specific tasks on account of the superposition state or entanglement. For these applications it is preferable to have spin centers connected both electronically and magnetically. Several vanadyl porphyrin dimers were studied recently and several of them presented interesting



**Citation:** Appleton, J.L.; Le Breton, N.; Choua, S.; Ruppert, R. The Effect of the Linking Unit on the Electronic and Magnetic Interactions in Copper(II) Porphyrin Dimers Linked by Metal Ions. *Inorganics* **2024**, *12*, 44. <https://doi.org/10.3390/inorganics12020044>

Academic Editor: Li Wang

Received: 18 December 2023

Revised: 19 January 2024

Accepted: 26 January 2024

Published: 27 January 2024



**Copyright:** © 2024 by the authors. Licensee MDPI, Basel, Switzerland. This article is an open access article distributed under the terms and conditions of the Creative Commons Attribution (CC BY) license (<https://creativecommons.org/licenses/by/4.0/>).

magnetic properties suitable for the development of two-qubit quantum gates [30–35]. The use of magnetic molecules for such applications appears to have merit as they are addressable objects of which the magnetic properties can be tuned. As the qubit is the fundamental component of the quantum computational device, a good understanding of its electronic and magnetic properties is of paramount importance.

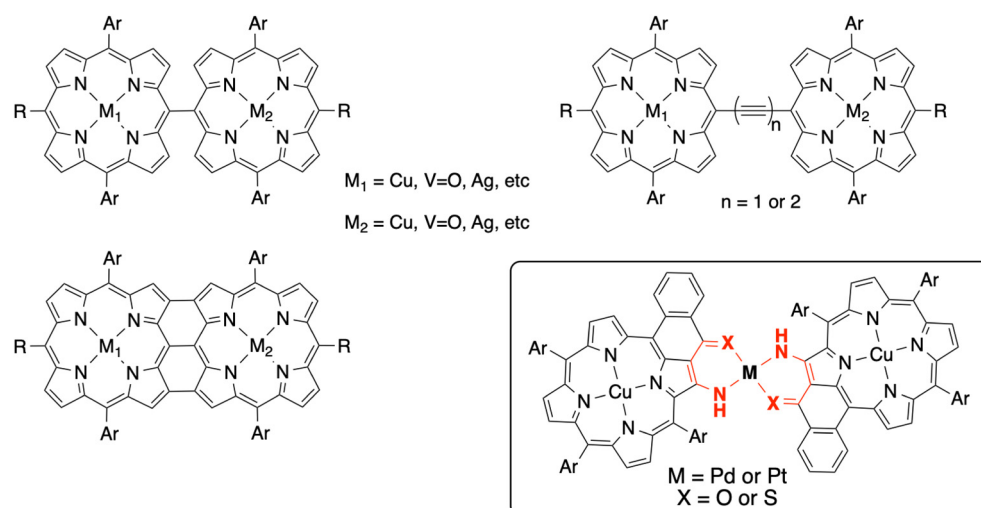


**Figure 1.** Several examples of porphyrin dimers prepared to study electronic and/or magnetic interactions between the two covalently linked metalloporphyrins. Insert: copper(II) porphyrin dimers studied in this report.

In porphyrin dimers linked by metal ions, we have shown before that efficient electronic communication was present in these dimers [36]. Porphyrins bearing different external coordination sites conjugated with the aromatic core have been prepared and used to generate a series of dimers or higher oligomers linked by different metal ions, in solution and on surfaces [37–39]. More recently, copper(II) or vanadyl porphyrin dimers were studied in our group, and an anti-ferromagnetic coupling was observed using EPR spectroscopy [40,41]. In this report, we describe the syntheses of new copper(II) porphyrin dimers, the effect of the linking unit (the coordination site nature and the linking metal ion) on the electronic and magnetic interactions between the two moieties (see Figure 1). The study of these interactions (electronic and magnetic) between two distant paramagnetic sites is of primary importance to the development of new efficient two-qubit systems.

## 2. Results and Discussion

### 2.1. Syntheses of the Compounds

The starting porphyrins were prepared by using classical Lindsey conditions [42] in a stoichiometric manner (see Figure 2). The reaction of three equivalents of benzaldehyde **1**, one equivalent of benzaldehyde **2**, and four equivalents of pyrrole in the presence of boron trifluoride as a Lewis acid led after oxidation with chloranil to a mixture of porphyrin bases, easily separated using column chromatography. Subsequent metalation with nickel(II) of the isolated free base gave the nickel(II) porphyrin **3** in 20% yield. After hydrolysis of the ester function, an intramolecular Friedel–Crafts reaction led to the extended nickel(II) porphyrin **4** in 79% yield. Then, **3** and **4** were obtained according to previously published synthetic pathways already reported in our group; the  $^1\text{H}$  and  $^{13}\text{C}$  NMR were identical to those of the already published porphyrins [43].

Nickel(II) porphyrin **4** was demetalated in a strong acidic medium (sulfuric acid and trifluoro acetic acid) and remetalated with copper(II) acetate to afford copper(II) porphyrin **5**. The external enamino-ketone coordination site was then created by reacting **5** with the Katritzky reagent to aminate the pyrrolic position next to the ketone [44]. Finally, the external coordination site was converted to the enaminothio-ketone by means of reaction

with Lawesson's reagent (see Figure 3) [45,46]. Copper(II) porphyrins **6** and **7** both had an external coordination site conjugated with the aromatic core of the macrocycle and were used to prepare porphyrin dimers linked by diamagnetic soft metal ions, in this study, palladium(II) and platinum(II).

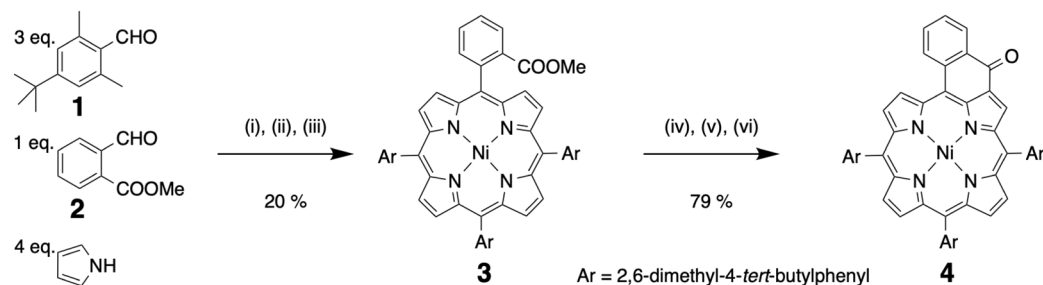


**Figure 2.** Synthesis of starting nickel(II) porphyrin **4**: (i)  $\text{BF}_3 \cdot \text{Et}_2\text{O}$ ,  $\text{CH}_2\text{Cl}_2$ ; (ii) chloranil; (iii)  $\text{Ni}(\text{acac})_2$ , toluene, reflux; (iv)  $\text{LiOH}$ , dioxane:water (8:2), reflux 16 h; (v) oxalyl chloride, toluene; (vi)  $\text{SnCl}_4$ , toluene RT, 30 min.

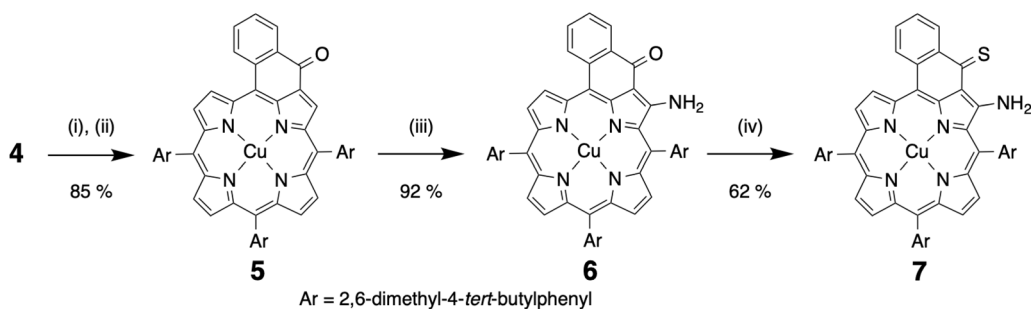


**Figure 3.** Synthesis of the two copper(II) porphyrins **6** and **7**. (i)  $\text{H}_2\text{SO}_4$ ,  $\text{CF}_3\text{COOH}$ ; (ii)  $\text{Cu}(\text{OAc})_2 \cdot \text{H}_2\text{O}$ , toluene, reflux; (iii) 4-Amino-4H-1,2,4-triazole,  $\text{NaOH}$ , toluene:ethanol (8:2), reflux; (iv) Lawesson's reagent, toluene, reflux.

These two copper(II) porphyrins were then reacted with two soft metal ions forming square planar complexes. Palladium(II) acetate and platinum(II) bis-acetylacetonate were the starting complexes used to generate porphyrin dimers **8**, **9**, **10**, and **11** (see Figure 4). The formation of the palladium(II) linked dimers was straightforward in refluxing toluene. The formation of the platinum(II) linked dimers was much more tedious and necessitated four days in refluxing 1,2-dichlorobenzene to reach reasonable yields starting from **6** (enaminoketone external site). The reaction conditions proved to be less harsh when starting from copper(II) porphyrin **7**, the soft enaminothioketone external site reacting much faster with the soft platinum(II) ion, with the dimer forming after 4 h at reflux.

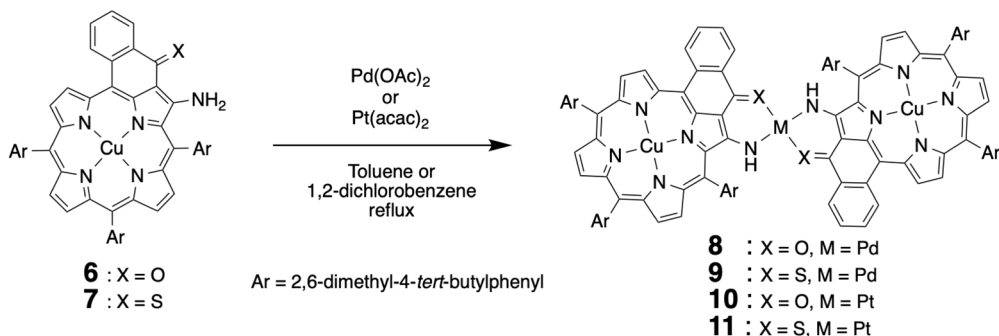


**Figure 4.** Syntheses of the copper(II) porphyrin dimers **8**, **9**, **10**, and **11**.

## 2.2. Electronic Interactions—Electrochemical Studies

The electronic properties of porphyrins, “the pigments of life” [47,48], are well documented because their occurrence and involvement in redox processes in nature have prompted many chemists to study the electrochemistry of such natural compounds and of many synthetic aromatic macrocycles [49,50]. In the case of copper(II) porphyrins, two reversible oxidation steps and two reversible reduction steps were generally observed [49,50], with the electron uptake or release being located on the aromatic macrocycle. The copper(II) ion generally remains formally in the oxidation state +2, as demonstrated by EPR spectroscopy.

The electronic spectra of the copper(II) porphyrins **6** and **7** were already bathochromically shifted compared to other porphyrins due to the extension of the aromatic macrocycle. The lowest energy bands were located at 660 nm and 717 nm, respectively, for **6** and **7** (see Figures 5 and 6, color curves). As observed earlier for other dimers [36], all bands of the new dimers were shifted to lower energies, the shift being even more pronounced in the case of the platinum(II) linkage (see Figure 5 for a comparison between compounds **6**, **8**, and **10**). Moving from 4 d to 5 d metal ions as linkers will lead to greater electronic communication and hence to a larger bathochromic shift (33 nm and 71 nm for **8** and **10**, respectively, with respect to **6**). A similar modification of the electronic spectra was observed for the enaminothioiketone series, once again on account of an increased orbital overlap between the linking unit and the metal ion. Bathochromic shifts of 20 nm and 80 nm were measured for dimers **9** and **11**, respectively, compared to copper(II) porphyrin **7** (see Figure 6).

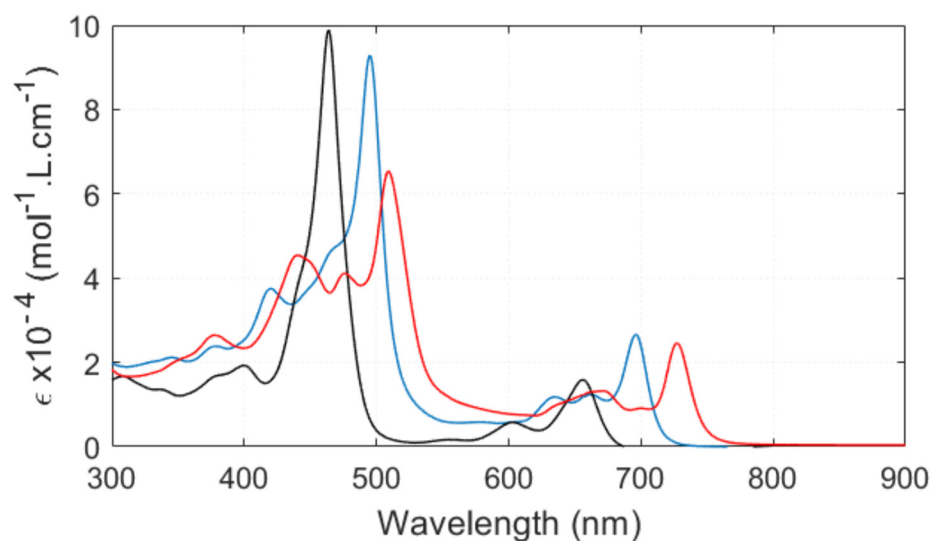


**Figure 5.** Electronic spectra of copper(II) porphyrin **6** (black) and of porphyrin dimers **8** (blue) and **10** (red) linked, respectively, by palladium(II) or platinum(II).

All compounds were studied by cyclic voltammetry; some results are summarized in Table 1, and a typical cyclic voltammetry is shown in Figure 7 (additional CVs can be found in Figures S8–S10). We had shown earlier that for these dimers linked by metal ions, the splitting of the redox processes occurred mainly on the oxidation side (see Figure 7 right). Generally, and contrarily to covalently conjugated dimers, on the reduction side, the reduction of the two copper(II) porphyrins took place at the same potentials in these dimers. With the exception of compound **7**, which adsorbed quite strongly on the electrode, rendering potential determination difficult, all other compounds presented reversible electronic exchanges, allowing easy comparison between the redox steps.

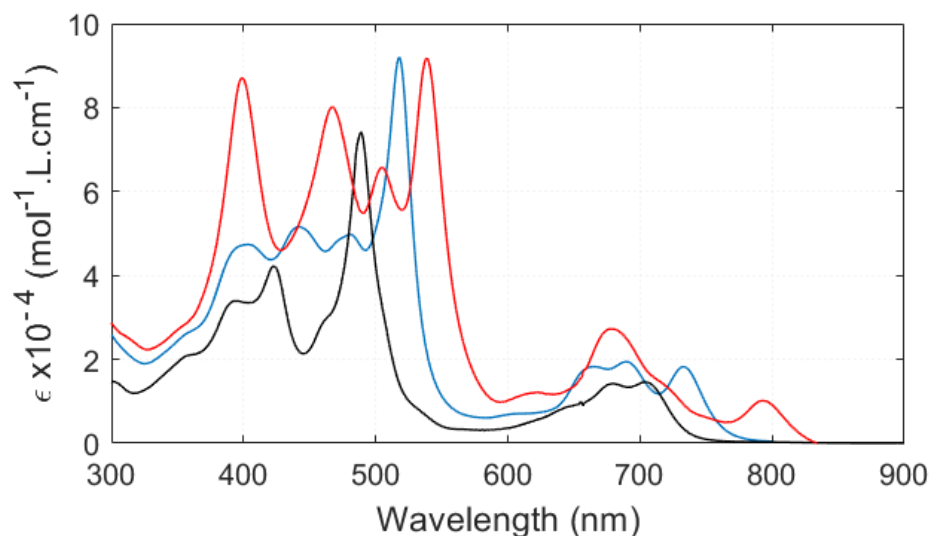


**Figure 6.** Electronic spectra of copper(II) porphyrin **7** (black) and of porphyrin dimers **9** (blue) and **11** (red) linked, respectively, by palladium(II) or platinum(II).

**Table 1.** Oxidation potentials of the porphyrin dimers obtained from cyclic voltammetric studies <sup>1</sup>.

Compound	$E_{Ox1}$ (Volt)	$E_{Ox2}$ (Volt)	$E_{Ox3}$ (Volt)	$E_{Ox2}-E_{Ox1}$ (mV)
<b>6</b>	0.47	0.82	-	-
<b>8</b>	0.29	0.43	0.77	140
<b>10</b>	0.28	0.49	0.85	209
<b>7</b>	-	-	-	-
<b>9</b>	0.26	0.50	0.83	237
<b>11</b>	0.23	0.54	0.90	310

<sup>1</sup>  $CH_2Cl_2$ ,  $NBu_4PF_6$ , (0.1 M), 100 mV/s vs.  $Fc^+/Fc$ , GC electrode.

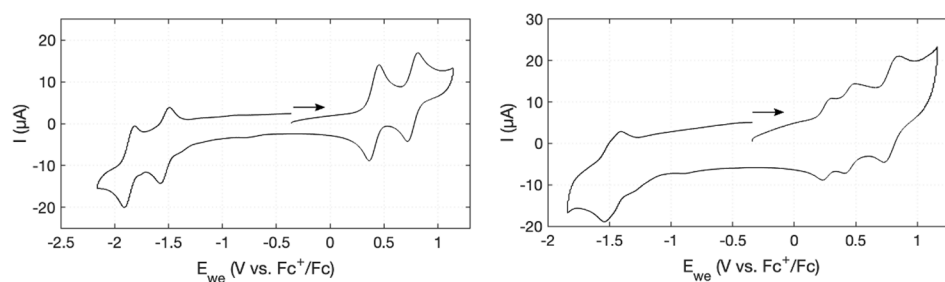


**Figure 7.** Cyclic voltammetry of **6** (left) and **10** (right) in dichloromethane with tetrabutylammonium hexafluorophosphate (0.1 M) at a scan rate of 100 mV/s. Arrow shows direction of the measurement.

The first oxidation potential was substantially lowered in dimers compared to the starting copper(II) porphyrin potentials, whereas the reduction potentials of the compounds were similar to the reduction potential of the monomer. Replacing the oxygen atom of the ketone with a sulfur atom increased markedly the splitting of the first oxidation waves, from a value of 140 mV to 237 mV in palladium(II) linked dimers and from 209 mV to 310 mV for the two platinum(II) linked dimers. “Significant splitting is a hallmark of strongly interacting ground-state redox centers and indicates that the resultant charge . . . is considerably delocalized over both porphyrin centers”: this was asserted by M. Therien in his seminal work in 1994. These splitting data can be compared to data reported for known covalently linked dimers. With one or two triple bonds as linking units between two zinc(II) porphyrins, Therien reported splitting values of 110 and 270 mV, respectively [12,51]. Later, for a triply fused copper(II) porphyrin dimer, the group of Osuka reported a value

of 390 mV [52]. It should be emphasized that the splitting values measured for these copper(II) porphyrin dimers are significantly larger than the values reported earlier for nickel(II) porphyrin dimers linked by palladium(II) or platinum(II) ions. The splitting values reported for the two platinum linked dimers with the enaminothioketone external sites were 290 mV and 310 mV, respectively, for the nickel(II) and the copper(II) porphyrins [53]. The lower splitting values of the nickel(II) porphyrins porphyrin dimers are probably due to the non-planarity of the nickel(II) porphyrins, compared to more planar copper(II) porphyrins [54]. The electronic delocalization is hence favored in the copper(II) porphyrin dimers described in this report, showing that the linking metal ions, the nature of the external coordination site, and also the metalloporphyrin used are of primary importance for efficient communication between the two aromatic moieties. This phenomenon has already been established by Osuka [52]. With the exception of compound 7 (adsorption problems in electrochemical studies), the electrochemical HOMO-LUMO gap (the potential difference between the first oxidation and the first reduction) correlated well with the values obtained from the lowest energy band in the electronic spectra.

For these dimers, the communication between the two porphyrins was present in the HOMO orbitals (participation of the d orbitals of the linking metal ions), but not in the LUMO (absence of communication through d orbitals), thus explaining why the splitting solely occurs during oxidation. We have described this effect earlier for other porphyrin dimers [53]. The relative atomic contributions to the HOMO of the bridging metal ions in dimers were calculated earlier and varied from 4.6% (PdNO dimer) to 11.2% (PtNO dimer) and 13.5% (PtNS dimer) in our energy transfer studies of zinc porphyrin-free base porphyrin dyads [53]. Consequently, the energy transfer rate was higher in dimers with 5 d linkers compared to the energy transfer rate in dimers with 4 d linking ions. The splitting of the first oxidation waves would increase in the same order ( $8 < 10 < 9 < 11$ ).

### 2.3. EPR Studies

The EPR spectrum of copper(II) porphyrin **6** is represented in Figure 8 and was similar to reported data for analogous compounds with different aromatic substituents [40]. The spectrum is characteristic of a copper(II) porphyrin with an almost axial shape and hyperfine coupling with one  $^{63,65}\text{Cu}$  ( $I = 3/2$ ) and four  $^{14}\text{N}$  ( $I = 1$ ). The unpaired electron of the copper metal ion is in a bonding orbital ( $d_{x^2-y^2}$ ), leading to good orbital overlap with the nitrogen atoms and, consequently, a well-resolved superhyperfine coupling interaction. The distance between two peaks is 17 G, which is around the expected value for hyperfine coupling with nitrogen atoms [55]. The simulated spectrum obtained by simulation using Easyspin [56] is presented in Figure 8 and was obtained using the parameters given in Table 2.

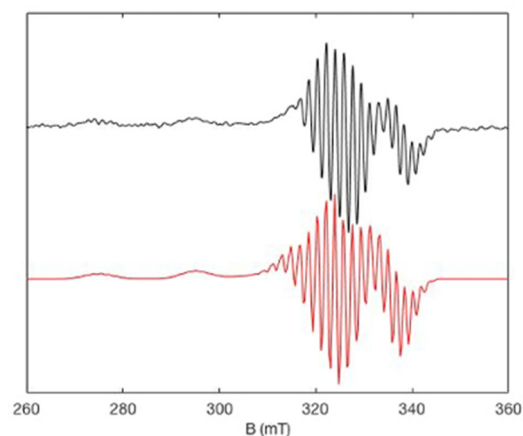


**Figure 8.** X-band experimental (black) and simulated (red) EPR spectra of copper(II) porphyrin **6** ( $10^{-4}$  M;  $\text{CH}_2\text{Cl}_2:\text{CHCl}_3$ ; 80:20) at 100 K, recorded with a microwave power of 0.5 mW and a modulation amplitude of 0.2 mT. Simulation parameters are given in Table 2.

**Table 2.** Best fit EPR parameters obtained for the simulation of the EPR spectra of copper(II) porphyrin **6** and of the four porphyrin dimers **8**, **10**, **9**, and **11** linked by palladium(II) and platinum(II).

	Compound <b>6</b>	Dimer <b>8</b> Pd <sub>NO</sub>	Dimer <b>10</b> Pt <sub>NO</sub>	Dimer <b>9</b> Pd <sub>NS</sub>	Dimer <b>11</b> Pt <sub>NS</sub>
$g_x$ (g strain)	2.061 (0.003)	2.061 (0.04)	2.061 (0.04)	2.061 (0.03)	2.061 (0.03)
$g_y$ (g strain)	2.051 (0.0075)	2.061 (0.04)	2.061 (0.04)	2.061 (0.03)	2.061 (0.03)
$g_z$ (g strain)	2.180 (0.001)	2.180 (0.07)	2.180 (0.07)	2.180 (0.05)	2.180 (0.05)
$A_{Cu}$ (MHz)	[135; 125; 600]	[130; 130; 600]	[130; 130; 600]	[130; 130; 600]	[130; 130; 600]
$A_N$ (MHz)	49	-	-	-	-
$ J $ (MHz)	-	$700 \pm 50$	$700 \pm 50$	$1500 \pm 200$	$1500 \pm 200$
$D$ (MHz)	-	$42 \pm 5$	$42 \pm 5$	$60 \pm 5$	$60 \pm 5$

The EPR spectrum of **8** suggests there was a weak magnetic interaction between the two paramagnetic metals. This can be visualized by comparing the EPR spectra of **6** and **8**, where the line broadening in the spectrum led to a loss of the hyperfine coupling and an intricate spectral pattern. The temperature variation also showed no spectral changes. The large distance between the two paramagnetic sites ( $\sim 14$  Å) impeded a strong  $J$  interaction, and the diamagnetic linking metal ion did not seem to act as a relay for magnetic communication [40]. The EPR spectrum can be analyzed as follows, where  $|J| < h\nu$  and the Hamiltonian described in Equation (1) can be used for the simulation.

$$\hat{H} = \mu_B \sum_{i=1}^2 \mathbf{Bg}_i^{Cu} \hat{S}_i^{Cu} + \sum_{i=1}^2 \hat{S}_i^{Cu} \mathbf{A}_i^{Cu} \hat{I}_i^{Cu} + \hat{S}_1^{Cu} \mathbf{J} \hat{S}_2^{Cu} \quad (1)$$

The  $\mathbf{J}$  interaction matrix comprises exchange and dipolar terms, each of which can be decomposed into isotropic, antisymmetric, and anisotropic components. Because our complex is almost perfectly centrosymmetric, we can use Moriya's principles to ignore the antisymmetric term, which means that  $\mathbf{J}$  may be expressed as the sum of the isotropic and anisotropic terms.

$$\mathbf{J} = J_{iso} S_1 S_2 + S_1 \mathbf{D}_{aniso} S_2 \quad (2)$$

$\mathbf{D}_{aniso}$  is a symmetric traceless tensor that represents the sum of eventual anisotropic exchange terms as well as dipolar interactions.

The experimental EPR spectrum of **10** (Figure 9) was similar to that of **8**, which was to be expected as they are both diamagnetic linkers, and there are few discrepancies between the two spectra. Superimposing the two spectra shows that the shape and line width were similar and, consequently, it can be assumed that the coupling in both the dimers was similar. The EPR parameters used for the simulation of the EPR spectrum of **10** are given in Table 2, and they are quite similar to the simulated parameters for **8**, demonstrating that the linking metal ion was not the determining point for the isotropic exchange coupling path. This means that changing the diamagnetic linking metal ion has a weak effect on the magnetic properties.

As well as an increased electronic interaction (vide supra), an increased magnetic interaction for the enaminothioketone porphyrin dimers (**9** and **11**) compared to the enaminothioketone porphyrin dimers (**8** and **10**) was also observed. Superimposing **10** and **11** showed differences (Figure 10), with a transition at high field ( $\sim 350$  mT) for **10**. This transition was present for **11** at a higher field ( $\sim 380$  mT), implying a stronger  $J$  coupling between the two paramagnetic metals for **11** compared to **10**, indicating differences in magnetic coupling on changing the external paramagnetic metal sites. The increased  $D$  value for the enaminothioketone simulated spectra compared to the enaminothioketone spectra showed that an anisotropic exchange coupling was also occurring.

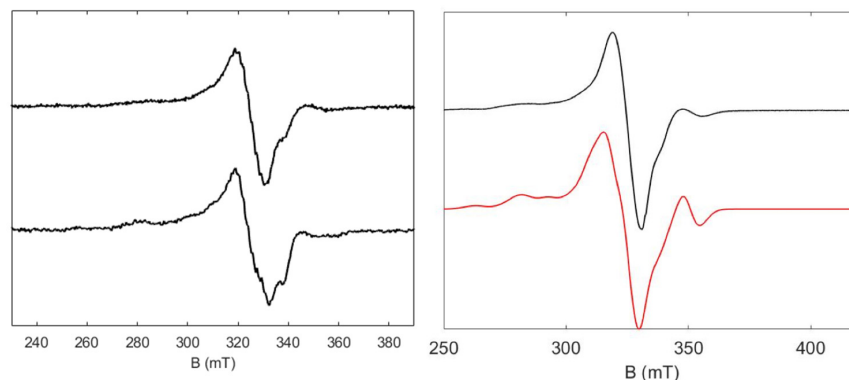


**Figure 9.** (Left): X-band experimental EPR spectrum of porphyrin dimer **8** (top) and **10** (bottom) ( $10^{-4}$  M;  $\text{CH}_2\text{Cl}_2:\text{CHCl}_3$ ; 80:20) 50 K, recorded with a microwave power of 0.1 mW and a modulation amplitude of 0.4 mT. (Right): experimental (black) and simulation (red) of compound **8** at 15 K. Simulation parameters are given in Table 2.

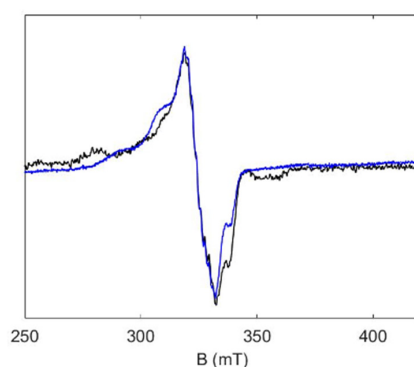


**Figure 10.** X-band experimental EPR spectrum showing a superposition of **10** (black) and **11** (blue) ( $10^{-4}$  M; 80:20;  $\text{CH}_2\text{Cl}_2:\text{CHCl}_3$ ) at 50 K recorded with a microwave power of 0.1 mW and a modulation amplitude of 0.4 mT.

In contrast, comparing the EPR spectrum of **9** and **11** (Figure 11) shows that the transitions and line width were essentially the same, as seen for **8** and **10** (vide supra). This demonstrates once again that varying the external metal ion from Pd(II) to Pt(II) has minimal effect on the magnetic properties. However, varying the external coordination site from an enaminoketone to an enaminothio ketone appears to increase the magnetic couplings between the two paramagnetic metal ions on account of a more efficient through-bond interaction.

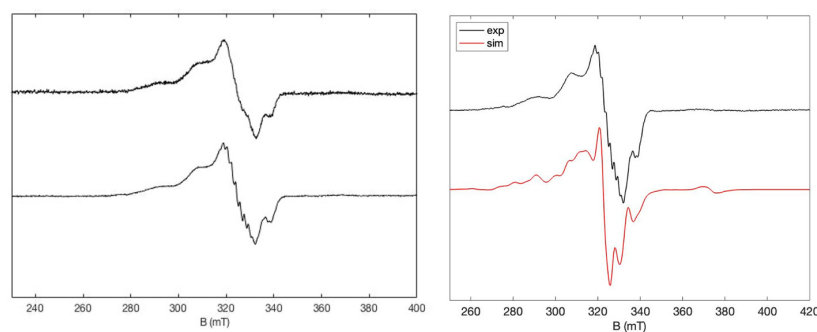


**Figure 11.** (Left): X-band experimental EPR spectrum of **9** (top) and **11** (bottom) ( $10^{-4}$  M; 80:20;  $\text{CH}_2\text{Cl}_2:\text{CHCl}_3$ ) at 15 K recorded with a microwave power of 0.1 mW and a modulation amplitude of 0.4 mT. (Right): experimental EPR spectrum of **11** at 50 K (black) and the corresponding simulation (red). Simulation parameters are given in Table 2.

### 3. Materials and Methods

All reagents and solvents were used as received on purchasing from commercial sources. 1-Bromo-4-*tert*-butyl-2,6-dimethylbenzene, [57] 2,6-dimethyl-4-*tert*-butylbenzaldehyde, [58] methyl-2-formylbenzoate [59], and nickel(II) and free base enaminoketone porphyrin [43] were prepared following previously published procedures. Distillations were carried out using sodium/benzophenone ketyl for toluene and calcium hydride for dichloromethane. Standard Schlenk techniques were employed to carry out most of the experiments under inert atmosphere. Merck (Darmstadt, Germany) silica gel (40–63  $\mu\text{m}$ ) was used for chromatographic separations.

A Bruker Avance 500 MHz spectrometer (Ettlingen, Karlsruhe, Germany) equipped with a cryoprobe was used to carry out  $^1\text{H}$  and  $^{13}\text{C}$  NMR in  $\text{CDCl}_3$  at 25 °C. Chemical shifts ( $\delta$  (ppm)) are shown relative to TMS. A Cary 5000 UV/vis/NIR double-beam spectrometer was used to record UV-visible spectra in dichloromethane. A Bruker Daltonics MicroTOF was used to collect ESI MS and a Bruker Autoflex II TOF-TOF instrument in positive ionization mode with dithranol as a matrix was used to collect MALDI MS; these measurements were carried out by S. Coutin (Service de Spectrométrie de Masse, Institut de Chimie, Université de Strasbourg). Elemental analysis was carried out by the Service d'Analyses de l'Institut de Chimie de Strasbourg (M. Heinrich, N. Bourgeois) using a ThermoFischer Scientific Flash2000. Electrochemical measurements were carried out using a glassy carbon working electrode with  $\text{NBu}_4\text{PF}_6$  (0.1 M) as the electrolyte and ferrocenium/ferrocene ( $\text{Fc}^+/\text{Fc}$ ) couple as an internal reference in distilled dichloromethane. The three electrodes were connected to a computerized electrochemical device (Biologic SP-150).

An EMXplus spectrometer (Bruker Biospin GmbH), equipped with an ESR900 continuous flow cryostat controlled with an Oxford ITC503S apparatus (Oxford Instrument) and a high sensitivity resonator (4119 HSW) was used to record X-band continuous-wave EPR spectra. Samples were introduced into 4 mm outer diameter clear fused quartz tube (Wilmad-LabGlass). The modulation frequency and amplitude were, respectively, of 100 kHz and 0.4 mT. The Bruker strong pitch ( $g = 2.0028$ ) was used to calibrate the  $g$  factor.

**Compound 5:** On demetallation of **4**, the free-base porphyrin (140 mg, 0.18 mmol) and an excess of  $\text{Cu}(\text{OAc})_2$  (85 mg, 0.47 mmol) were refluxed in toluene (50 mL) for 16 h. The solvent was evaporated, and the product was purified using column chromatography ( $\text{SiO}_2$ ; dichloromethane:cyclohexane 1:1) followed by precipitation to afford the titled product (141 mg, 0.17 mmol, 94%). MALDI-TOF: Calcd for  $\text{C}_{63}\text{H}_{62}\text{N}_4\text{OCu}$  ( $\text{M}^{\bullet+}$ ) 954.43; obsd 954.391.

**Compound 6:** compound **5** (173 mg, 0.181 mmol), 4-amino-4H-1,2,4-triazole (304 mg, 3.62 mmol) and NaOH (724 mg, 18.1 mmol) were refluxed for 2 h in toluene:ethanol (8:2) under argon. Water (50 mL) was then added and the organic phase was washed with water and dried over sodium sulphate. The solvent was evaporated, and the porphyrin was purified using column chromatography ( $\text{SiO}_2$ ; dichloromethane:cyclohexane 2:1) to afford the titled product (161 mg, 0.167 mmol, 92%). HR-ESI: Calcd for  $\text{C}_{63}\text{H}_{63}\text{N}_5\text{OCu}$  ( $\text{M}^+$ ) 968.4312; obsd 968.4323. Elemental analysis: calcd %N 7.22% C 78.03% H 6.55. obsd %N 7.15% C 77.68% H 6.60.

**Compound 7:** compound **6** (65 mg, 0.067 mmol) and Lawesson's reagent (162 mg, 0.402 mmol) were heated to reflux in toluene for 2 h under argon. On cooling, the solvent was evaporated, and the product was purified using column chromatography ( $\text{SiO}_2$ ; cyclohexane:dichloromethane 1:1) to afford the titled product (57 mg, 0.058 mmol, 86%). MALDI-TOF: Calcd for  $\text{C}_{63}\text{H}_{63}\text{N}_5\text{OCu}$  ( $\text{M} + \text{H}^+$ ) 985.42; obsd 985.447

**Compound 8:** compound **6** (35 mg, 0.036 mmol) and  $\text{Pd}(\text{OAc})_2$  (4 mg, 0.018 mmol) were heated to reflux in toluene (20 mL) for 16 h under argon. On cooling, the solvent was evaporated, and the product was purified using column chromatography ( $\text{SiO}_2$ ; cyclohexane:dichloromethane 60:40) to afford the titled product as a brown solid (13 mg, 6.4  $\mu\text{mol}$ , 36%). MALDI-TOF: Calcd for  $\text{C}_{126}\text{H}_{124}\text{N}_{10}\text{O}_2\text{PdCu}_2$  ( $\text{M}^{\bullet+}$ ) 2040.75; obsd 2040.924.

**Compound 10:** compound **6** (10 mg, 0.01 mmol) and  $\text{Pt}(\text{acac})_2$  (2 mg, 5.6  $\mu\text{mol}$ ) were heated to reflux in 1,2-dichlorobenzene for 4 days under argon. On cooling, the solvent

was evaporated using trap-to-trap distillation, and the product was purified using column chromatography (SiO<sub>2</sub>; cyclohexane:dichloromethane 60:40) to afford the titled product as a brown solid (2 mg, 0.94 μmol, 18%). MALDI-TOF: Calcd for C<sub>126</sub>H<sub>124</sub>N<sub>10</sub>O<sub>2</sub>PdCu<sub>2</sub> (M<sup>•+</sup>) 2132.62; obsd 2132.901.

Compound **9**: compound **7** (15 mg, 0.016 mmol) and Pd(OAc)<sub>2</sub> (2 mg, 8.6 μmol) were heated to reflux in toluene for 1 h under argon. On cooling, the solvent was evaporated, and the product was purified using column chromatography (SiO<sub>2</sub>; cyclohexane:dichloromethane 1:1) to afford the titled product (5 mg, 2.4 μmol, 57%). MALDI-TOF: Calcd for C<sub>126</sub>H<sub>124</sub>N<sub>10</sub>S<sub>2</sub>PdCu<sub>2</sub> (M<sup>•+</sup>) 2072.71; obsd 2072.117.

Compound **11**: compound **7** (8 mg, 8.4 μmol) and Pt(acac)<sub>2</sub> (1.8 mg, 4.6 μmol) were heated to reflux in 1,2-dichlorobenzene for 4 h under argon. On cooling, the solvent was evaporated using trap-to-trap distillation, and the product was purified using column chromatography (SiO<sub>2</sub>; cyclohexane:dichloromethane 1:1) to afford the titled product as a deep red solid (4 mg, 1.89 μmol, 45%). MALDI-TOF: Calcd for C<sub>126</sub>H<sub>124</sub>N<sub>10</sub>S<sub>2</sub>PtCu<sub>2</sub> (M<sup>•+</sup>) 2161.77; obsd 2161.712.

#### 4. Conclusions

This study showed that electronic interaction within porphyrin dimers can be modulated by changing the connecting metal ions between the two porphyrins, the nature of the external coordination site, and the metal ion in the porphyrin core. An increase in the electronic communication between the two porphyrin moieties could be observed on switching the external metal ion from Pd(II) to Pt(II) and/or switching the linking unit from an enamino-ketone to an enaminothio-ketone. This could be evidenced by using electronic spectroscopy and cyclic voltammetry. Furthermore, it was possible to see small but measurable changes in the magnetic interactions between two paramagnetic centers separated by rather long distances close to 14 Å, on varying the linking moiety. Work in progress concerns magnetic interactions in homo- and hetero-dinuclear porphyrin dimers for potential uses in quantum information processing.

**Supplementary Materials:** The following supporting information can be downloaded at: <https://www.mdpi.com/article/10.3390/inorganics12020044/s1>, Figure S1: MALDI Mass spectroscopy of **5** (top) and a zoom of the spectrum (bottom); Figure S2: MALDI Mass spectroscopy of **6** (top) and a zoom of the spectrum (bottom); Figure S3: MALDI Mass spectroscopy of **7** (top) and a zoom of the spectrum (bottom); Figure S4: MALDI Mass spectroscopy of **8** (top) and a zoom of the spectrum (bottom); Figure S5: MALDI Mass spectroscopy of **10** (top) and a zoom of the spectrum (bottom); Figure S6: MALDI Mass spectroscopy of **9** (top) and a zoom of the spectrum (bottom); Figure S7: MALDI Mass spectroscopy of **11** (top) and a zoom of the spectrum (bottom); Figure S8: cyclic voltammetry of **8** in dichloromethane with tetrabutylammonium hexafluorophosphate (0.1 M) at a scan rate of 100 mV/s. Arrow shows direction of the measurement; only the oxidation is shown to emphasise the splitting; Figure S9: cyclic voltammetry of **9** in dichloromethane with tetrabutylammonium hexafluorophosphate (0.1 M) at a scan rate of 100 mV/s. Arrow shows direction of the measurement; only the oxidation is shown to emphasise the splitting; Figure S10: cyclic voltammetry of **11** in dichloromethane with tetrabutylammonium hexafluorophosphate (0.1 M) at a scan rate of 100 mV/s. Arrow shows direction of the measurement; only the oxidation is shown to emphasise the splitting; Figure S11: X-band experimental EPR spectrum of porphyrin dimer **8** (10<sup>-4</sup> M; CH<sub>2</sub>Cl<sub>2</sub>:CHCl<sub>3</sub>; 80:20) at 15 K and 50 K, recorded with a microwave power of 0.1 mW and a modulation amplitude of 0.4 mT; Figure S12: X-band experimental EPR spectra of **10** (10<sup>-4</sup> M; CH<sub>2</sub>Cl<sub>2</sub>:CHCl<sub>3</sub>; 80:20) at 4 K and 50 K recorded with a microwave power of 0.1 mW and a modulation amplitude of 0.4 mT; Figure S13: X-band experimental EPR spectrum of porphyrin dimer **9** (10<sup>-4</sup> M; CH<sub>2</sub>Cl<sub>2</sub>:CHCl<sub>3</sub>; 80:20) at 50 K, recorded with a microwave power of 0.1 mW and a modulation amplitude of 0.4 mT and the corresponding simulation (red). Simulation parameters are given in Table 2; Figure S14: X-band experimental EPR spectra of **9** (10<sup>-4</sup> M; CH<sub>2</sub>Cl<sub>2</sub>:CHCl<sub>3</sub>; 80:20) at 5 K and 50 K recorded with a microwave power of 0.1 mW and a modulation amplitude of 0.4 mT; Figure S15: X-band experimental EPR spectra of **11** (10<sup>-4</sup> M; CH<sub>2</sub>Cl<sub>2</sub>:CHCl<sub>3</sub>; 80:20) at 5 K and 50 K recorded with a microwave power of 0.1 mW and a modulation amplitude of 0.4 mT; Figure S16: X-band experimental EPR spectrum of

porphyrin dimer 10 ( $10^{-4}$  M;  $\text{CH}_2\text{Cl}_2:\text{CHCl}_3$ ; 80:20) at 50 K, recorded with a microwave power of 0.1 mW and a modulation amplitude of 0.4 mT and the corresponding simulation (red). Simulation parameters are given in Table 2.

**Author Contributions:** Conceptualization, S.C. and R.R.; methodology, S.C. and R.R.; software, S.C., J.L.A. and N.L.B.; investigation, J.L.A. and N.L.B.; writing—original draft preparation, R.R. and S.C.; writing—review and editing, J.L.A., N.L.B., S.C. and R.R.; supervision, S.C. and R.R.; project administration, R.R.; funding acquisition, R.R. and S.C. All authors have read and agreed to the published version of the manuscript.

**Funding:** The authors gratefully acknowledge the University of Strasbourg and the CNRS for continuous financial support. J.L.A. thanks the French Ministry of Research for his Ph.D. fellowship.

**Data Availability Statement:** The data presented in this study are available in this article.

**Acknowledgments:** The authors gratefully acknowledge the University of Strasbourg and the CNRS for continuous financial support. J.L.A. thanks the French Ministry of Research for his Ph.D. fellowship.

**Conflicts of Interest:** The authors declare no conflicts of interest.

## References

1. Kadish, K.M.; Smith, K.M.; Guillard, R. (Eds.) *The Porphyrin Handbook*; Academic Press: San Diego, CA, USA, 2000; Volumes 1–7.
2. Zhang, Y.; Lovell, J.F. Porphyrins as theranostic agents from prehistoric to modern times. *Theranostics* **2012**, *2*, 905–915. [[CrossRef](#)]
3. Josefsen, L.B.; Boyle, R.W. Unique diagnostic and therapeutic roles of porphyrins and phthalocyanines in photodynamic therapy, imaging and theranostics. *Theranostics* **2012**, *2*, 916–966. [[CrossRef](#)]
4. Li, L.-L.; Diau, E.W.-G. Porphyrin-sensitized solar cells. *Chem. Soc. Rev.* **2013**, *42*, 291–304. [[CrossRef](#)]
5. Higashino, T.; Imahori, H. Porphyrins as excellent dyes for dye-sensitized solar cells: Recent developments and insights. *Dalton Trans.* **2015**, *44*, 448–463. [[CrossRef](#)]
6. Urbani, M.; Grätzel, M.; Nazeeruddin, M.K.; Torres, T. Meso-substituted porphyrins for dye-sensitized solar cells. *Chem. Rev.* **2014**, *114*, 12330–12396. [[CrossRef](#)] [[PubMed](#)]
7. Senge, M.O. Stirring the porphyrin alphabet soup—Functionalization reactions for porphyrins. *Chem. Commun.* **2011**, *47*, 1943–1960. [[CrossRef](#)] [[PubMed](#)]
8. Hiroto, S.; Miyake, Y.; Shinokubo, H. Synthesis and functionalization of porphyrins through organometallic methodologies. *Chem. Rev.* **2017**, *117*, 2910–3043. [[CrossRef](#)] [[PubMed](#)]
9. Harriman, A.; Sauvage, J.-P. A strategy for constructing photosynthetic models: Porphyrin-containing modules assembled around transition metals. *Chem. Soc. Rev.* **1996**, *25*, 41–48. [[CrossRef](#)]
10. Crossley, M.J.; Burn, P.L. Rigid, laterally-bridged bis-porphyrin system. *J. Chem. Soc. Chem. Commun.* **1987**, 39–40. [[CrossRef](#)]
11. Anderson, H.L. Conjugated porphyrin ladders. *Inorg. Chem.* **1994**, *33*, 972–981. [[CrossRef](#)]
12. Lin, V.S.-Y.; DiMagno, S.G.; Therien, M.J. Highly conjugated, acetylenyl bridged porphyrins: New models for light-harvesting antenna systems. *Science* **1994**, *264*, 1105–1111. [[CrossRef](#)]
13. Jaquinod, L.; Siri, O.; Khoury, R.G.; Smith, K.M. Linear fused oligoporphyrins: Potential molecular wires with enhanced electronic communication between bridged metal ions. *Chem. Commun.* **1998**, 1261–1262. [[CrossRef](#)]
14. Mori, H.; Tanaka, T.; Osuka, A. Fused porphyrinoids as promising near-infrared absorbing dyes. *J. Mater. Chem. C* **2013**, *1*, 2500–2519. [[CrossRef](#)]
15. Tanaka, T.; Osuka, A. Conjugated porphyrin arrays: Synthesis, properties and applications for functional materials. *Chem. Soc. Rev.* **2015**, *44*, 943–969. [[CrossRef](#)]
16. Tsuda, A.; Osuka, A. Fully conjugated porphyrin tapes with electronic absorption bands that reach into infrared. *Science* **2001**, *293*, 79–82. [[CrossRef](#)]
17. Kahn, O. *Molecular Magnetism*; VCH: New York, NY, USA, 1993.
18. Kobayashi, N.; Numao, N.; Kondo, R.; Nakajima, S.; Osa, T. A planar binuclear tetrabenzoporphyrin and its dicopper derivative. *Inorg. Chem.* **1991**, *30*, 2241–2244. [[CrossRef](#)]
19. Ikeue, T.; Furukawa, K.; Hata, H.; Aratani, N.; Shinokubo, H.; Kato, T.; Osuka, A. The importance of a  $\beta$ – $\beta$  bond for long-range antiferromagnetic coupling in directly linked copper(II) and silver(II) diporphyrins. *Angew. Chem. Int. Ed.* **2005**, *44*, 6899–6901. [[CrossRef](#)]
20. Toganoh, M.; Furuta, H. Blooming of confused porphyrinoids—fusion, expansion, contraction and more confusion. *Chem. Commun.* **2012**, *48*, 937–954. [[CrossRef](#)] [[PubMed](#)]
21. Wang, R.; Brugh, A.M.; Rawson, J.; Therien, M.J.; Forbes, M.D.E. Alkyne-bridged multi[copper(II) porphyrin] structures: Nuances of orbital symmetry in long-range, through-bond mediated, isotropic spin exchange interactions. *J. Am. Chem. Soc.* **2017**, *139*, 9759–9762. [[CrossRef](#)]

22. Wang, R.; Ko, C.-H.; Brugh, A.M.; Bai, Y.; Forbes, M.D.E.; Therien, M.J. Topology, distance, and orbital symmetry effects on electronic spin-spin couplings in rigid molecular systems: Implications for long-distance spin-spin interactions. *J. Phys. Chem. A* **2020**, *124*, 7411–7415. [[CrossRef](#)]
23. Brugh, A.M.; Wang, R.; Therien, M.J.; Forbes, M.D.E. Spinning molecules, spinning spins: Modulation of an electron spin exchange interaction in a highly anisotropic hyperfine field. *ACS Omega* **2021**, *6*, 27865–27873. [[CrossRef](#)] [[PubMed](#)]
24. Richert, S.; Kuprov, I.; Peeks, M.D.; Suturina, E.A.; Cremers, J.; Anderson, H.L.; Timmel, C.R. Quantifying the exchange coupling in linear copper porphyrin oligomers. *Phys. Chem. Chem. Phys.* **2017**, *19*, 16057–16061. [[CrossRef](#)]
25. Leznoff, C.C.; Lam, H.; Marcuccio, S.M.; Nevin, W.A.; Janda, P.; Kobayashi, N.; Lever, A.B.P. A planar binuclear phthalocyanine and its dicobalt derivatives. *J. Chem. Soc. Chem. Commun.* **1987**, 699–701. [[CrossRef](#)]
26. Lelièvre, D.; Bosio, L.; Simon, J.; André, J.-J.; Bensebaa, F. Dimeric substituted copper phthalocyanine liquid crystals. Synthesis, characterization and magnetic properties. *J. Am. Chem. Soc.* **1992**, *114*, 4475–4479. [[CrossRef](#)]
27. Zhao, M.; Stern, C.; Barrett, A.G.M.; Hoffman, B.M. Porphyrazines as molecular scaffolds: Periphery-core spin coupling between metal ions of a Schiff base porphyrazine. *Angew. Chem. Int. Ed.* **2003**, *42*, 462–465. [[CrossRef](#)] [[PubMed](#)]
28. Matano, Y.; Fujii, D.; Shibano, T.; Furukawa, K.; Higashino, T.; Nakano, H.; Imahori, H. Covalently linked 5,15-diazaporphyrin dimers: Promising scaffolds for a highly conjugated azaporphyrin  $\pi$  system. *Chem. Eur. J.* **2014**, *20*, 3342–3349. [[CrossRef](#)] [[PubMed](#)]
29. Chmielewski, P.J. Lucky seven: Characterization of stable T-shaped copper(II) complexes of [32]heptaphyrins. *Angew. Chem. Int. Ed.* **2010**, *49*, 1359–1361. [[CrossRef](#)]
30. Gaita-Arino, A.; Luis, F.; Hill, S.; Coronado, E. Molecular spins for quantum computation. *Nat. Chem.* **2019**, *11*, 301–309. [[CrossRef](#)]
31. Atzori, M.; Tesi, L.; Morra, E.; Chiesa, M.; Sorace, L.; Sessoli, R. Room-temperature quantum coherence and Rabi oscillations in vanadyl phthalocyanine: Toward multifunctional molecular spin qubits. *J. Am. Chem. Soc.* **2016**, *138*, 2154–2157. [[CrossRef](#)]
32. Von Kugelgen, S.; Krzyaniak, M.D.; Gu, M.; Puggioni, D.; Rondinelli, J.M.; Wasielewski, M.R.; Freedman, D.E. Spectral Addressability in a Modular Two Qubit System. *J. Am. Chem. Soc.* **2021**, *143*, 8069–8077. [[CrossRef](#)]
33. Ranieri, D.; Santanni, F.; Privitera, A.; Albino, A.; Salvadori, E.; Chiesa, M.; Totti, F.; Sorace, L.; Sessoli, R. An exchange coupled *meso-meso* linked vanadyl porphyrin dimer for quantum information processing. *Chem. Sci.* **2023**, *14*, 61–69. [[CrossRef](#)]
34. Pozo, I.; Huang, Z.; Lombardi, F.; Alexandropoulos, D.I.; Kong, F.; Slota, M.; Tkach, I.; Bennati, M.; Deng, J.-R.; Stawski, W.; et al. Enhanced coherence by coupling spins through a delocalized-system: Vanadyl porphyrin dimers. *Chem* **2024**, *10*, 299–316. [[CrossRef](#)]
35. Ranieri, D.; Privitera, A.; Santanni, F.; Urbanska, K.; Strachan, G.J.; Twanley, B.; Salvadori, E.; Liao, Y.-K.; Chiesa, M.; Senge, M.O.; et al. A heterometallic porphyrin dimer as a potential quantum gate: Magneto-structural correlations and spin coherence properties. *Angew. Chem. Int. Ed.* **2023**, *62*, e202312936. [[CrossRef](#)]
36. Richeter, S.; Jeandon, C.; Gisselbrecht, J.-P.; Ruppert, R.; Callot, H.J. Syntheses and optical and electrochemical properties of porphyrin dimers linked by metal ions. *J. Am. Chem. Soc.* **2002**, *124*, 6168–6179. [[CrossRef](#)] [[PubMed](#)]
37. Wytko, J.A.; Ruppert, R.; Jeandon, C.; Weiss, J. Metal-mediated linear self-assembly of porphyrins. *Chem. Commun.* **2018**, *54*, 1550–1558. [[CrossRef](#)] [[PubMed](#)]
38. Carvalho, M.-A.; Dekkiche, H.; Karmazin, L.; Sanchez, F.; Vincent, B.; Kanesato, M.; Kikkawa, Y.; Ruppert, R. Synthesis and study at a solid/liquid interface of porphyrin dimers linked by metal ions. *Inorg. Chem.* **2017**, *56*, 15081–15090. [[CrossRef](#)] [[PubMed](#)]
39. Carvalho, M.-A.; Dekkiche, H.; Nagasaki, M.; Kikkawa, Y.; Ruppert, R. Coordination-driven construction of porphyrin nanoribbons at a highly oriented pyrolytic graphite (HOPG)/liquid interface. *J. Am. Chem. Soc.* **2019**, *141*, 10137–10141. [[CrossRef](#)] [[PubMed](#)]
40. Carvalho, M.-A.; Dekkiche, H.; Richeter, S.; Bailly, C.; Karmazin, L.; McKearney, D.; Leznoff, D.B.; Rogez, G.; Vileno, B.; Choua, S.; et al. Antiferromagnetic coupling in copper(II)-porphyrin dimers linked by copper(II) or palladium(II) ion. *J. Porphyr. Phthalocyanines* **2020**, *24*, 238–246. [[CrossRef](#)]
41. Appleton, J.L.; Le Breton, N.; Carvalho, M.-A.; Weiss, J.; Boudalis, A.K.; Gourlaouen, C.; Choua, S.; Ruppert, R. Vanadyl(IV) porphyrin dimers with palladium(II) and platinum(II) linkages: Syntheses, electronic properties, and magnetic interactions between the two moieties. *Cryst. Growth Des.* **2023**, *23*, 1689–1696. [[CrossRef](#)]
42. Lindsey, J.S.; Schreiman, I.C.; Hsu, H.C.; Kearney, P.C.; Marguerettaz, A.M. Rothmund and Adler-Longo reactions revisited: Synthesis of tetraphenylporphyrins under equilibrium conditions. *J. Org. Chem.* **1987**, *52*, 827–836. [[CrossRef](#)]
43. Dekkiche, H.; Carvalho, M.-A.; Jeandon, C.; Karmazin, L.; Boudon, C.; Ruhlmann, L.; Ruppert, R. Synthesis and electrochemistry of nickel(II)porphyrins bearing external palladium(II) or platinum(II) complexes. *J. Porphyr. Phthalocyanines* **2021**, *25*, 1133–1142. [[CrossRef](#)]
44. Katritzky, A.R.; Laurenzo, K.S. Direct amination of nitrobenzenes by vicarious nucleophilic substitution. *J. Org. Chem.* **1986**, *51*, 5039–5040. [[CrossRef](#)]
45. Pedersen, B.S.; Scheibye, S.; Nilsson, N.H.; Lawesson, S.-O. Studies on organophosphorus compounds XX. Syntheses of thioketones. *Bull. Soc. Chim. Belg.* **1978**, *87*, 223–228. [[CrossRef](#)]
46. Scheibye, S.; Pedersen, B.S.; Lawesson, S.-O. Studies on organophosphorus compounds XXI. The dimer of p-methoxyphenylthionophosphine sulfide as thiation reagent. A new route to thiocarboxamides. *Bull. Soc. Chim. Belg.* **1978**, *87*, 229–238. [[CrossRef](#)]
47. Battersby, A.R. Tetrapyrroles: The pigments of life. *Nat. Prod. Rep.* **2000**, *17*, 507–526. [[CrossRef](#)] [[PubMed](#)]

48. Anderson, H.L. Building molecular wires from the colours of life: Conjugated porphyrin oligomers. *Chem. Commun.* **1999**, 2323–2330. [[CrossRef](#)]
49. Kadish, K.M.; Royal, G.; Van Caemelbecke, E.; Gueletti, L. *The Porphyrin Handbook*; Kadish, K.M., Smith, K.M., Guillard, R., Eds.; Academic Press: San Diego, CA, USA, 2000; Volume 9, pp. 1–219.
50. Kadish, K.M.; Van Caemelbecke, E.; Royal, G. *The Porphyrin Handbook*; Kadish, K.M., Smith, K.M., Guillard, R., Eds.; Academic Press: San Diego, CA, USA, 2000; Volume 8, pp. 1–114.
51. Lin, V.S.-Y.; Therien, M.J. The role of porphyrin-to-porphyrin linkage topology in the extensive modulation of the absorptive and emissive properties of a series of ethynyl- and butadiynyl-bridged bis- and tris(porphinato)zinc chromophores. *Chem. Eur. J.* **1995**, *1*, 645–651. [[CrossRef](#)]
52. Tsuda, A.; Furuta, H.; Osuka, A. Syntheses, structural characterizations, and optical and electrochemical properties of directly fused diporphyrins. *J. Am. Chem. Soc.* **2001**, *123*, 10304–10321. [[CrossRef](#)] [[PubMed](#)]
53. Dekkiche, H.; Buisson, A.; Langlois, A.; Karsenti, P.-L.; Ruhlmann, L.; Harvey, P.D.; Ruppert, R. Ultrafast singlet energy transfer in porphyrin dyads. *Inorg. Chem.* **2016**, *55*, 10329–10336. [[CrossRef](#)]
54. Senge, M.O. X-ray data of porphyrins, see for example. In *The Porphyrin Handbook*; Kadish, K.M., Smith, K.M., Guillard, R., Eds.; Academic Press: San Diego, CA, USA, 2000; Volume 10, pp. 1–218.
55. Zhao, M.; Zhong, C.; Stern, C.; Barrett, A.G.M.; Hoffman, B.M. Synthesis and Magnetic Properties Comparison of M-Cu(II) and M-VO(II) Schiff Base-Porphyrazine Complexes: What Is the Mechanism for Spin-Coupling? *J. Am. Chem. Soc.* **2005**, *127*, 9769–9775. [[CrossRef](#)]
56. Stoll, S.; Schweiger, A. EasySpin, a comprehensive software package for spectral simulation and analysis in EPR. *J. Magn. Reson.* **2006**, *178*, 42–55. [[CrossRef](#)] [[PubMed](#)]
57. Field, J.E.; Hill, T.J.; Venkataraman, D. Bridged Triarylamines: A New Class of Heterohelicenes. *J. Org. Chem.* **2003**, *68*, 6071–6078. [[CrossRef](#)] [[PubMed](#)]
58. Ito, S.; Hiroto, S.; Lee, S.; Son, M.; Hisaki, I.; Yoshida, T.; Kim, D.; Kobayashi, N.; Shinokubo, H. Synthesis of highly twisted and fully p-conjugated porphyrinic oligomers. *J. Am. Chem. Soc.* **2015**, *137*, 142–145. [[CrossRef](#)] [[PubMed](#)]
59. Osuka, A.; Nakajima, S.; Maruyama, K. Synthesis of a 1,2-phenylene-bridged triporphyrin. *J. Org. Chem.* **1992**, *57*, 7355–7359. [[CrossRef](#)]

**Disclaimer/Publisher's Note:** The statements, opinions and data contained in all publications are solely those of the individual author(s) and contributor(s) and not of MDPI and/or the editor(s). MDPI and/or the editor(s) disclaim responsibility for any injury to people or property resulting from any ideas, methods, instructions or products referred to in the content.